Video Article

Visualization of Motor Axon Navigation and Quantification of Axon Arborization In Mouse Embryos Using Light Sheet Fluorescence Microscopy

Ee Shan Liau*[1,2], Ya-Ping Yen*[2,3], Jun-An Chen[1,2]

[1]Molecular and Cell Biology, Taiwan International Graduate Program, Academia Sinica and Graduate Institute of Life Sciences, National Defense Medical Center

[2]Institute of Molecular Biology, Academia Sinica

[3]Institute of Biotechnology, College of Bio-Resources and Agriculture, National Taiwan University

*These authors contributed equally

Correspondence to: Jun-An Chen at jachen@imb.sinica.edu.tw

URL: https://www.jove.com/video/57546
DOI: doi:10.3791/57546

Keywords: Neuroscience, Issue 135, Motor neuron, axon navigation, axon trajectory, axon arborization, light sheet microscopy, spinal cord, IMARIS

Date Published: 5/11/2018

Citation: Liau, E.S., Yen, Y.P., Chen, J.A. Visualization of Motor Axon Navigation and Quantification of Axon Arborization In Mouse Embryos Using Light Sheet Fluorescence Microscopy. *J. Vis. Exp.* (135), e57546, doi:10.3791/57546 (2018).

Abstract

Spinal motor neurons (MNs) extend their axons to communicate with their innervating targets, thereby controlling movement and complex tasks in vertebrates. Thus, it is critical to uncover the molecular mechanisms of how motor axons navigate to, arborize, and innervate their peripheral muscle targets during development and degeneration. Although transgenic *Hb9::GFP* mouse lines have long served to visualize motor axon trajectories during embryonic development, detailed descriptions of the full spectrum of axon terminal arborization remain incomplete due to the pattern complexity and limitations of current optical microscopy. Here, we describe an improved protocol that combines light sheet fluorescence microscopy (LSFM) and robust image analysis to qualitatively and quantitatively visualize developing motor axons. This system can be easily adopted to cross genetic mutants or MN disease models with *Hb9::GFP* lines, revealing novel molecular mechanisms that lead to defects in motor axon navigation and arborization.

Video Link

The video component of this article can be found at https://www.jove.com/video/57546/

Introduction

Spinal MNs are the part of the central nervous system but innervate peripheral muscles to control movement. In the developing spinal cord, MN progenitors (pMNs) are established according to the signals emanating from the notochord and adjacent somites. All differentiated post-mitotic MNs are then generated from pMNs, eventually giving rise to a series of MN subtypes along the rostrocaudal axis of the spinal cord[1,2]. Spinal MNs are topographically and anatomically well organized. Their morphological arrangement correlates with the position of their respective target in the periphery[3]. Upon reaching their muscle targets, axons receive cellular and exogenous neurotrophic factors that induce them to extend and branch further into muscles. Innervation and branching defects may contribute to the failure to form neuromuscular junctions (NMJ). For example, glial-derived neurotrophic factors (GDNF)-induced Pea3 is indispensable for axon arborization into cutaneous maximus (CM) and latissimus dorsi (LD) muscles[4,5]. In addition, *DINE* knockout mouse embryos show defective arborization of phrenic nerves in the diaphragm, causing respiratory failure and mortality immediately after birth[6,7]. Therefore, this last step of MN maturation (*i.e.*, axonal projection and branching) is critical to ensure communication between neurons and target cells.

To view arborization patterns, researchers normally conduct confocal imaging or two-photon fluorescence light microscopy of sectioned or whole-mount samples[8,9,10]. Both of these microscopy techniques generate acceptable resolution and depth penetration. Two-photon fluorescence light microscopy involves excitation of fluorophores by simultaneous absorption of two lower-energy photons[11]. Since two-photon excitation uses near-infrared radiation, the decreased excitation frequency contributes to reduced scattering and better tissue penetration up to 1 mm in tissue, thus allowing imaging with greater depth. Confocal microscopy removes by filters the out-of-focus signals and only collects light within the focal plane[12]. With this approach, images of samples from different focal planes can be combined to produce a three-dimensional (3D) image via a Z-stack function. Nevertheless, signal intensity is reduced as most of the light is blocked and high numerical apertures obscure the depth-of-field. More importantly, both techniques contribute to the severe photodamage and phototoxicity since the whole specimen receives illumination even when only one plane is imaged at a given time.

To circumvent these shortcomings, LSFM has become a favored alternative, with the advantages of being fast, light-efficient, and less phototoxic[13,14]. In addition, LSFM allows multi-view imaging. This approach is particularly suited to visualizing motor axons and their dispersing terminals as they spread through 3D space. LSFM outperforms the other two options because samples are mounted on a stage that allows rotation around a vertical axis and movements along the x, y, and z axes. This set-up not only allows for a minimally blocked view of the sample but also the choice of a desirable illumination path, a shortcoming of two-photon and confocal microscopy, both of which require mounting of

Copyright © 2018 Journal of Visualized Experiments

samples on a flat slide. Therefore, LSFM is the most suitable tool for 3D imaging of axon arborization and for quantification of motor nerve terminals in mouse embryos.

Protocol

All of the live animals were kept in a specific pathogen free (SPF) animal facility, approved and overseen by IACUC of Academia Sinica.

1. Fixation

1. Collect embryos of embryonic day 12.5 (E12.5) then decapitate and eviscerate them.
2. Fix the embryos individually in 24-well plates with 1 mL/well of freshly prepared 4% paraformaldehyde in 1x phosphate buffer saline (PBS) overnight. Incubate at 4 °C on a shaker.
3. Wash the fixed embryos at least 3x, each for 5-10 min, with 1 mL of 1x PBS and incubate overnight at 4 °C on a shaker to remove the residual paraformaldehyde.

2. Whole-mount Immunostaining

1. Permeabilize each embryo in 1 mL of 0.5% PBS-Triton-X-100 (PBST) overnight at 4 °C on a shaker.
2. Block each sample with 1 mL of 10% FBS prepared in 1x PBS overnight at 4 °C on a shaker.
3. Incubate the embryo with 1 mL of anti-GFP primary antibody (1:1,000 dilution in 10% FBS) at 4 °C for 72 h with constant shaking to intensify the GFP signal of motor nerves.
4. After the primary antibody incubation, wash with 1 mL of 0.5% PBST over the course of 1-2 days at 4 °C on a shaker, changing the 0.5% PBST at least three times.
5. Apply 1 mL of secondary antibody (1:1,000 dilution in 10% FBS) and incubate overnight in the dark at 4 °C with constant shaking.
6. Wash 3x with 1 mL of 0.5% PBST at 4 °C on a shaker over the course of 2-3 days. Keep samples in 1x PBS at 4 °C until the day before imaging.
   NOTE: Embryos can be dissected into smaller segments before clearing, depending on which part of the embryos will be imaged. Forelimbs are preserved in this experimental approach (**Figure 1A**).
7. Incubate the embryo in a commercial clearing reagent with a refractive index of 1.49 nD in a 1.5 mL tube, protected from light at room temperature overnight, to render the embryo transparent for imaging.
   NOTE: The volume of the clearing reagent is approximately five times that of the sample volume.

3. LSFM (2–3 h)

1. **Sample set-up**
   1. Set up 5X/0.1 illumination optics and 5X/0.16 detection optics. Assemble the sample holder and sample capillary (1.5 mm internal diameter, green) and place them into the microscope.
      NOTE: Refer to the microscope's Operating Manual for detailed set-up procedures.
   2. Mount the embryo as follows:
      1. Prepare the P200 pipette tip by cutting away the upper part so that it fits the diameter of the capillary and remove the pointed part (~ 3 mm) for the sample attachment.
      2. Melt the blunted end of the pipette tip using a small flame.
      3. Extinguish the flame and quickly attach the embryo vertically onto the melted end.
      4. Fit the upper part of the pipette tip with the sample capillary.
   3. Allow the chamber buffer to equilibrate with the embryo for 1 min to clear off debris or bubbles.
   4. Using the imaging software, select **Locate capillary** under the **Locate** tab and adjust the x, y, z axes to position the sample capillary.
   5. Select **Locate sample** and zoom to 0.6X to focus on the embryo. Rotate the embryo to ensure that the long axis of the imaged limb aligns with the light path of the two light sources (**Figure 1B**).

2. **Image acquisition**
   1. Under the **Acquisition** tab, define the light path parameters such as detection objectives, laser blocking filter, beam splitter, cameras, and lasers.
      NOTE: The GFP channel is used in this experiment (Excitation wavelength: 488 nm; emission filter: BP 505 to 545 nm, beam splitter: SPS LP 560).
   2. Check the pivot scan checkbox for shadow reduction.
   3. Define the acquisition settings: bit depth, 16 bit; zoom, 0.36-0.7X; single-side illumination (left/right) or dual-side illumination.
   4. Click **Continuous** and set the laser intensity, exposure time, laser power, and light sheet position to acquire sharper images.
      NOTE: The laser power is kept as low as possible to minimize photodamage.
   5. Press **STOP** to end image acquisition.

3. **Multidimensional acquisition**
   1. Define the z-stack by moving the Z position for the first and last image. Click **Optimal** to set the slice number.
   2. Click **Start Experiment** to acquire the selected z-stack.
   3. When it is done, save the image in .czi format.

4. **Image processing (optional)**

Copyright © 2018 Journal of Visualized Experiments

1. Proceed with **Dual side fusion** under the **Lightsheet Processing** channel if dual-side illumination is applied. **Multiview processing** is necessary if multi-views are acquired to combine images from multiple angles.
2. Create a 2D image using data from the highest intensity pixels along the projection axis under the **Maximum Intensity Projection** channel.
3. Under **Copy** channel, click **Subset** to select subsets of images from the original set.

4. Quantification of Axon Arborization (30 Min for Each Individual Nerve)

1. Open the image file in the imaging analysis software (by default, the image containing the XYZ data is opened in Surpass mode and as a 3D-rendered view).
2. Adjust the image color, brightness, and contrast using the **Display Adjustment** window (**Edit | Show Display Adjustment**) to detect filaments based on local intensity contrast.
3. Click on the **Add New Filaments** icon and select the **Autopath (no loop)** algorithm in the drop-down menu.
4. Select the region of interest (in this case, the segmenting axon of interest). Click **Next** when finished.
5. Define the starting and seed points by assigning the largest and thinnest diameter measurements, which can be measured using the **Slice** mode.
6. Assign a starting point at the edge of the region of interest. To achieve manual addition or removal of starting points, first change the pointer mode (**Navigate | Select**) and then **Shift + right-click** at the points of interest.
7. Select manual thresholds for seed points to ensure that all of the visible arborization is marked. Change the pointer mode (**Navigate | Select**) and then **Shift + left-click** at the points of interest to manually add or remove seed points.
   NOTE: It is important to manually remove background noises and signals from neighboring nerves.
8. Check the box **Remove seed points around starting points**.
9. Check **Remove disconnected segments** to allow exclusion of points that are too far away and that may represent background noise. Indicate the **Maximum Gap Length** in the next step to define the upper limit for exclusion.
10. Adjust the threshold for background subtraction, which uses a Gaussian filter to estimate the background intensity of every voxel.
11. Set automatic threshold for dendrite diameter using the **Approximate cross-section area** algorithm.
12. Skip the steps for spine calculation.
13. Finish the process and choose the desired style and color.
14. Uncheck the volume box in **Properties** to view only the reconstructed axons.
15. Under the **Statistics** tab, select **Detailed**. Use **Filament No. Dendrite Terminal Points** to quantify the motor nerve terminals as an indicator of motor axon arborization.
    NOTE: Statistical annotation can be added if desired.
16. Export the image of the reconstructed axon as a .tif file.

Representative Results

LSFM provides detailed 3D visualization of MN trajectory and axon arborization in mouse embryos. Under bright field, tissues appear completely transparent after being immersed in the commercial clearing reagent. No shrinkage or swelling of the sample was noticed after up to one week of storage in clearing reagent before imaging. Under fluorescence channel, motor neurons are labeled with transgenically expressed GFP (**Movie 1**). In some instance, details of the axon structure are compromised. For example, **Figure 2** represents low quality imaging. Several factors can impede imaging quality. Firstly, insufficient permeabilization and washing steps can lead to high background signal. Secondly, light scattering through inadequately cleared tissue will result in blurred images. Lastly, suboptimal sample positioning during image acquisition might increase light scattering or block the light path.

To image axon arborization in greater detail and to perform quantification, magnification can be adjusted so that every finely arborized structure can be revealed (**Movie 2**). Images of single- and dual-side illumination should be compared to determine the optimal resolution of arborization pattern (**Figure 3**). Imaging analysis software can then be used to reconstruct axon arborization patterns for individual forelimb nerves (**Figure 4**). By defining the starting point and the diameter for seed point detection, these arborized structures can be semi-automatically detected and computed while background signals are manually removed. We used the "Filament - No. Dendrite Terminal Pts" function mode to calculate the total motor nerve terminals of individual nerves as an indicator of motor axon arborization. Additionally, branch length, mean diameter, and volume can be calculated using "Filament - Dendrite Length", "Filament - Dendrite Mean Diameter" and "Filament - Dendrite Volume", respectively.

Copyright © 2018 Journal of Visualized Experiments

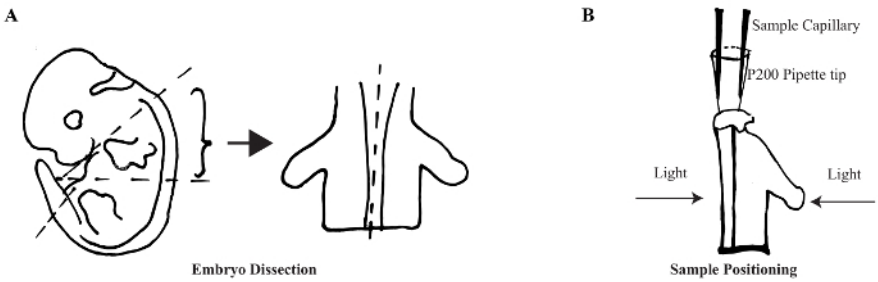

Figure 1: Graphical illustration of sample set-up. (**A**) During sample preparation, embryos are first decapitated and eviscerated. Forelimbs are dissected along the dashed line. (**B**) In the sample chamber, samples are positioned to keep the whole region of interest along the light path. Please click here to view a larger version of this figure.

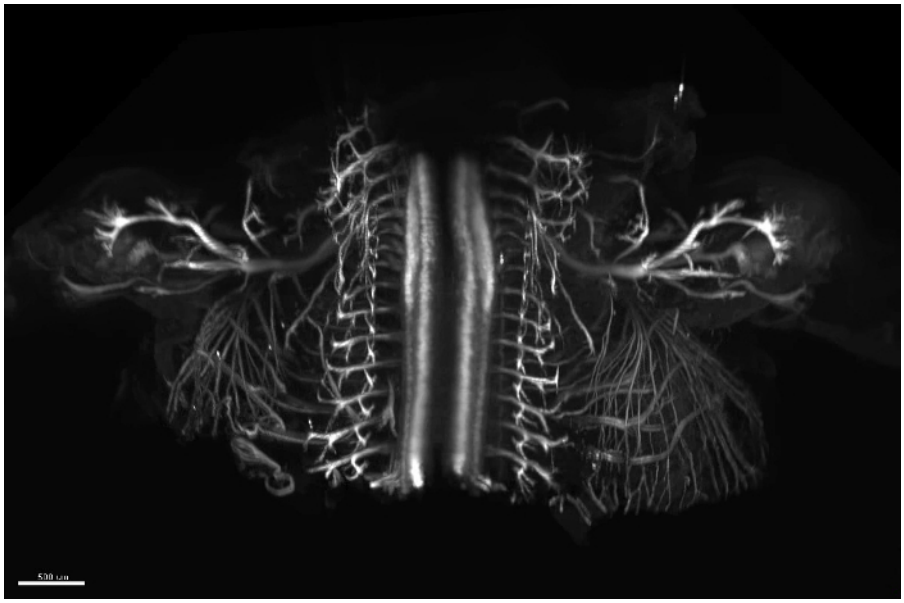

Movie 1: Light sheet fluorescence microscopy of a large field of view of the upper half of an E12.5 transgenic mouse embryo (*Hb9::GFP*). The movie clearly demonstrates motor nerves projecting from the spinal cord to their innervating targets. The 3D image is first acquired under 0.3X magnification with single-side illumination and 30 ms exposure time and later is processed into video using image analysis software. Scale bar represents 500 µm. Please click here to view this video. (Right-click to download.)

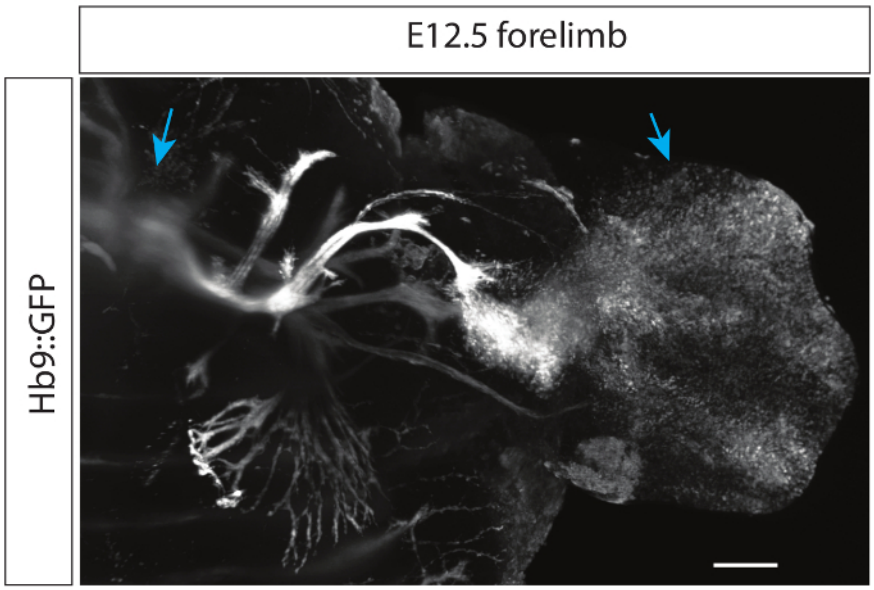

Figure 2: Example of a low-quality image with high background signal and blurred regions (blue arrows). The improper steps during sample preparation and image acquisition may lead to the impaired image quality to jeopardize the accuracy of any subsequent quantification of axon arborization. Scale bar in the image represents 200 µm. Please click here to view a larger version of this figure.

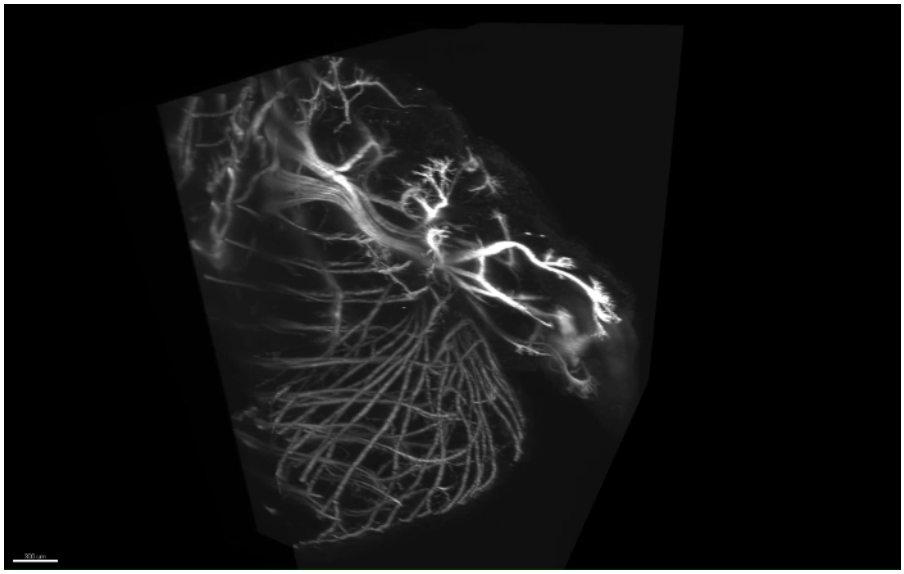

Movie 2: Visualization of E12.5 forelimb nerves under 488 nm excitation with dual-side illumination at a magnification of 0.6X. The zoomed-in movie allows clear and panoramic visualization of every fine arborized structures on individual nerves. Scale bar represents 300 µm. Please click here to view this video. (Right-click to download.)

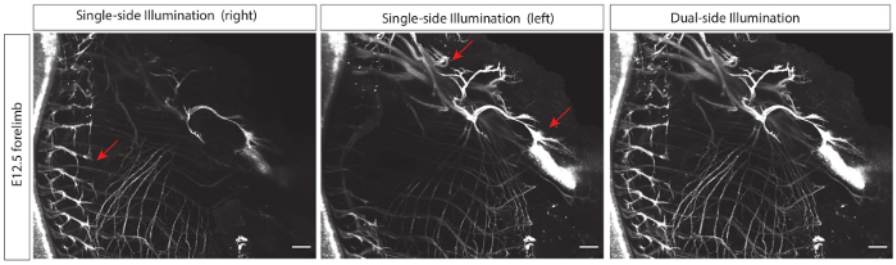

Figure 3: Comparison between single- and dual-side illumination. Both left and right illuminations display details of certain regions only (red arrows), whereas a combined image from dual-side illuminations provides a more complete view of the arborization pattern. However, single-side illumination can be achieved in a shorter imaging time and sometimes with better image quality. This is due to the fact that illumination paths from both sides may not lie perfectly on a single plane, resulting in blurring during dual-side illuminations. Images are shown as maximum intensity projection. Scale bar represents 200 µm. Please click here to view a larger version of this figure.

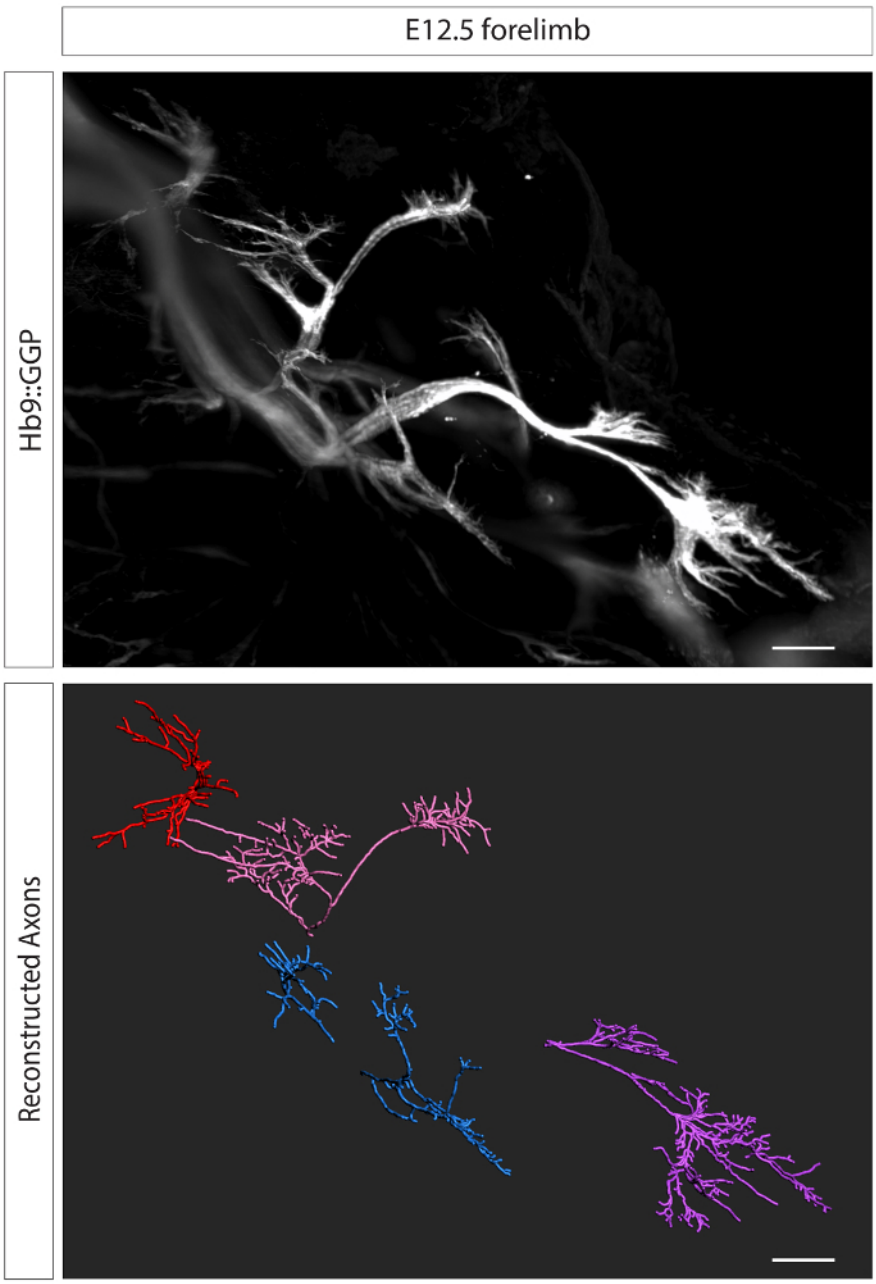

Figure 4: Reconstructed axon arborization of individual forelimb nerves, color-coded as follows: suprascapular (red), axillary (pink), radial (blue), posterior brachial cutaneous (purple). Arborization complexity was calculated according to the number of terminal end-points detected using our semi-automated method. The Autopath (no loop) algorithm traces filaments and detects seed points from user-defined starting points. Scale bar in both images represents 200 µm. Please click here to view a larger version of this figure.

Discussion

Several steps in the protocol may be subjected to changes under certain circumstances. For example, the duration of fixation depends on the age of the embryos, varying from 2 h to 1 or more days using freshly-made paraformaldehyde. Since fixation is carried out prior to whole mount immunostaining, for antibodies that are sensitive to protein crosslinking, methanol can be used as an alternative fixative agent. For a high signal-to-noise ratio upon staining, it is necessary to optimize the detergent concentration (between 0.1-0.5%). Additional washing steps before and after antibody incubation can also increase the signal-to-noise ratio. In addition, a tissue-clearing step is important to ensure that the light path is unblocked throughout deep axonal projections. To enhance tissue transparency, it is important to ensure minimal introduction of PBS during incubation in the commercial clearing agent, as the clearing effect is reversed by re-immersing samples in buffer solutions. Otherwise, a clearing reagent with a higher refractive index or a longer clearing period is recommended. Meanwhile, parameters during image acquisition vary among different samples. Dual-side illumination and multiview imaging may allow imaging with greater depth-of-field and enhanced detail. However,

Copyright © 2018 Journal of Visualized Experiments

since illumination from different angles is acquired simultaneously, single-side illumination is more efficient for smaller specimens or moving samples. A good quality image ensures accuracy for the following quantitative analyses.

Previous studies, including those by our group, have utilized either confocal imaging or two-photon microscopy to observe the motor axon navigation process or arborization pattern in *Hb9::GFP* embryos[10,15,16,17]. Based on our experience, we believe LSFM to be superior to these other two methods since: 1) Imaging time is largely reduced as LSFM offers more rapid and higher quality imaging, whilst minimizing photodamage and phototoxicity of samples. Specimens are illuminated from the side with a thin light sheet, thereby creating an intrinsic optical section[14,18,19]. The center of the light sheet converges with the focal plane of the detection system, which is orthogonal to the illumination axis. Consequently, out-of-focus light is reduced and only fluorophores within the focal plane are illuminated for every image, *i.e.*, rather than the entire specimen, thereby reducing photobleaching[20]. 2) Details of the arborization pattern are much better illustrated as LSFM allows multiview imaging. Instead of the specimen being mounted onto a slide, it is attached in such a way that rotation around a vertical axis is possible, as are movements along the x, y, and z dimensions. The images from the different planes and views are stacked to produce more isotropic 3D images. However, LSFM also has a limitation compared to confocal and two-photon approaches in terms of the massive file size created for each image. These pros and cons need to be weighed when deciding which imaging method to use, but ultimately the choice will depend on which microscopic hardware/software is available upon request.

In short, this protocol combines whole-mount immunostaining, state-of-the-art light sheet 3D imaging, together with quantification in image analysis software. We believe this protocol not only provides a new paradigm for visualizing motor axon navigation and trajectories in embryos with quantitation of axon arborization complexity but could also be applied to other neuron systems (*i.e.*, sensory neurons) with appropriate transgenic mice.

Disclosures

The authors have nothing to disclose.

Acknowledgements

LSFM experiments and data analysis were performed in part using the advanced optical microscopes of the Division of Instrument Service in Academia Sinica and with the assistance of Ms. Shu-Chen Shen. We thank Ms. Sue-Ping Lee from the Imaging Core Facility of IMB for considerable technical assistance with Imaris image analysis. The IMB's Scientific English Editing Core reviewed the manuscript. This work is funded by Academia Sinica Career Development Award (CDA-107-L05), MoST (104-2311-B-001-030-MY3), and NHRI (NHRI-EX106-10315NC).

References

1. Davis-Dusenbery, B. N., Williams, L. A., Klim, J. R., & Eggan, K. How to make spinal motor neurons. *Development.* **141**, 491-501 (2014).
2. Stifani, N. Motor neurons and the generation of spinal motor neuron diversity. *Front Cell Neurosci.* **8**, 293 (2014).
3. Kania, A., & Jessell, T. M. Topographic motor projections in the limb imposed by LIM homeodomain protein regulation of ephrin-A:EphA interactions. *Neuron.* **38**, 581-596 (2003).
4. Livet, J. *et al.* ETS gene Pea3 controls the central position and terminal arborization of specific motor neuron pools. *Neuron.* **35**, 877-892 (2002).
5. Kanning, K. C., Kaplan, A., & Henderson, C. E. Motor neuron diversity in development and disease. *Annu Rev Neurosci.* **33**, 409-440 (2010).
6. Matsumoto, S., Kiryu-Seo, S., & Kiyama, H. Motor Nerve Arborization Requires Proteolytic Domain of Damage-Induced Neuronal Endopeptidase (DINE) during Development. *J Neurosci.* **36**, 4744-4757 (2016).
7. Nagata, K. *et al.* ECEL1 mutation implicates impaired axonal arborization of motor nerves in the pathogenesis of distal arthrogryposis. *Acta Neuropathol.* **132**, 111-126 (2016).
8. Catela, C., Shin, M. M., Lee, D. H., Liu, J. P., & Dasen, J. S. Hox Proteins Coordinate Motor Neuron Differentiation and Connectivity Programs through Ret/Gfralpha Genes. *Cell Rep.* **14**, 1901-1915 (2016).
9. Bonanomi, D. *et al.* Ret is a multifunctional coreceptor that integrates diffusible- and contact-axon guidance signals. *Cell.* **148**, 568-582 (2012).
10. Tung, Y. T. *et al.* Mir-17 approximately 92 Governs Motor Neuron Subtype Survival by Mediating Nuclear PTEN. *Cell Rep.* **11**, 1305-1318 (2015).
11. Svoboda, K., & Yasuda, R. Principles of two-photon excitation microscopy and its applications to neuroscience. *Neuron.* **50**, 823-839 (2006).
12. Jonkman, J., & Brown, C. M. Any Way You Slice It-A Comparison of Confocal Microscopy Techniques. *J Biomol Tech.* **26**, 54-65 (2015).
13. Reynaud, E. G., Peychl, J., Huisken, J., & Tomancak, P. Guide to light-sheet microscopy for adventurous biologists. *Nat Methods.* **12**, 30-34 (2015).
14. Santi, P. A. Light sheet fluorescence microscopy: a review. *J Histochem Cytochem.* **59**, 129-138 (2011).
15. Hanley, O. *et al.* Parallel Pbx-Dependent Pathways Govern the Coalescence and Fate of Motor Columns. *Neuron.* **91**, 1005-1020 (2016).
16. De Marco Garcia, N. V., & Jessell, T. M. Early motor neuron pool identity and muscle nerve trajectory defined by postmitotic restrictions in Nkx6.1 activity. *Neuron.* **57**, 217-231 (2008).
17. Li, C. J. *et al.* MicroRNA filters Hox temporal transcription noise to confer boundary formation in the spinal cord. *Nat Commun.* **8**, 14685 (2017).
18. Swoger, J., Pampaloni, F., & Stelzer, E. H. Light-sheet-based fluorescence microscopy for three-dimensional imaging of biological samples. *Cold Spring Harb Protoc.* **2014**, 1-8 (2014).
19. Pantazis, P., & Supatto, W. Advances in whole-embryo imaging: a quantitative transition is underway. *Nat Rev Mol Cell Biol.* **15**, 327-339 (2014).
20. Reynaud, E. G., & Tomancak, P. Meeting report: first light sheet based fluorescence microscopy workshop. *Biotechnol J.* **5**, 798-804 (2010).

Copyright © 2018 Journal of Visualized Experiments